An analysis of subgrid-scale interactions in numerically simulated isotropic turbulence

J. Andrzej Domaradzki and Wei Liu
Department of Aerospace Engineering, University of Southern California, Los Angeles, California 90089-1191

Marc E. Brachet
Laboratoire de Physique Statistique, École Normale Supérieure, 75231 Paris Cedex 05, France

(Received 20 August 1992; accepted 15 March 1993)

Using a velocity field obtained in a direct numerical simulation of isotropic turbulence at moderate Reynolds number the subgrid-scale energy transfer in the spectral and the physical space representation is analyzed. The subgrid-scale transfer is found to be composed of a forward and an inverse transfer component, both being significant in dynamics of resolved scales. Energy exchanges between the resolved and unresolved scales from the vicinity of the cutoff wave number dominate the subgrid-scale processes and the energetics of the resolved scales are unaffected by the modes with wave numbers greater than twice the cutoff wave number. Correlations between the subgrid-scale transfer and the large-scale properties of the velocity field are investigated.

I. INTRODUCTION

Three approaches used in numerical predictions of turbulent flows are direct numerical simulations (DNS), large eddy simulations (LES), and Reynolds-averaged Navier–Stokes (RANS) simulations. With currently available computer capabilities the applicability of the DNS methods is limited to low Reynolds number turbulence. In practical applications for high Reynolds number flows the RANS techniques are used most frequently. The main drawback of this method is the need for introduction of a number of phenomenological closure assumptions and empirical, flow-dependent constants.

The LES techniques, reviewed by Rogallo and Moin[1] and more recently by Lesieur,[2] are a compromise approach between DNS and RANS. In the LES large, resolved scales of a turbulent flow are simulated directly, akin to the DNS approach, and their interactions with the small, unresolved scales are modeled like in the RANS approach. However, contrary to the RANS, only a part of the nonlinear interactions is modeled in the LES, and since the modeled interactions involve small scales (usually in the inertial range of turbulence) which have more universal character than flow-dependent large scales, the hope is that such modeling can be accomplished with less empiricism and with greater help from the theories of homogeneous turbulence than is the case for the RANS approach. At the present time the most widely used subgrid-scale models are the Smagorinsky model[3] for the LES performed in the physical space representation and the Kraichnan[4] and the Cholet and Lesieur models[5] if the spectral representation is used. These, as well as other subgrid-scale models, despite exhibiting a number of desirable properties like accounting properly for the global energy flux from the large to the small scales, are known to be deficient in some respects. For instance, the models are usually purely dissipative. However, the process of the subgrid-scale energy transfer is dissipative only in the mean and locally in the spectral or the physical space the effect of the subgrid-scale interactions may be to either decrease or increase the energy of the large, resolved scales. Various attempts were proposed in the past to account for the inverse energy transfer in the subgrid-scale modeling for homogeneous turbulence[6–8] and for inhomogeneous flows[9] but no generally accepted method exists.

The practical importance of the LES techniques and the deficiencies of the existing subgrid-scale models suggest that better understanding of subgrid-scale interactions is needed if improvements in the LES methods are to be made. To compute the effects of the subgrid-scale nonlinear interactions a full velocity field in three-space dimensions must be known; such detailed information cannot be obtained using current experimental techniques. Required information, however, is available in the direct numerical simulations of turbulent flows and has been used in the past to investigate the subgrid-scale interactions and to assess directly the validity of the models. Such an approach was pioneered by Clark *et al.*[10] for the physical space modeling and by Domaradzki *et al.*[11] for the spectral space modeling. A major limitation of this approach is that only low Reynolds number flows can be simulated numerically and thus it is unclear to what extent conclusions from such analyses are applicable to the more important case of high Reynolds number turbulence.

In this work we investigate the properties of the subgrid-scale nonlinear interactions using both the physical and the spectral space representation for numerically simulated, decaying homogeneous turbulence. The simulated flow is the Taylor–Green vortex and using its symmetries[12] it is possible to increase Reynolds number by a factor of 2 as compared with the general nonsymmetric flows simulated with the same number of computational modes. It is hoped that the higher Reynolds number and the existence of a short inertial subrange for this flow can make results of such an investigation applicable to high Reynolds number turbulence.

 0899-8213/93/5(7)/1747/13/$6.00

II. NUMERICAL SIMULATIONS

The Taylor–Green vortex flow[13] develops from the following initial condition:

$$u=\sin(x)\cos(y)\cos(z),$$
$$v=-\cos(x)\sin(y)\cos(z), \qquad (1)$$
$$w=0.$$

At time $t=0$ the flow is two dimensional but becomes three dimensional for all times $t>0$ when it develops into initially well-organized, laminar structures in the form of vortex sheets which subsequently become unstable resulting eventually in a fully turbulent flow. It was noted by Orszag[12] that the initial condition (1) has a number of symmetries which are consistent with symmetries of the Navier–Stokes equations and are thus preserved in time as flow evolves. In the context of spectral simulations the symmetries of the flow may then be used to reduce the number of computational modes needed to describe the flow for a prescribed range of resolved scales. This idea was implemented by Brachet *et al.*[14] who were able to simulate the Taylor–Green vortex flow with an effective spatial resolution of 256^3 modes at a computer cost equivalent to simulating a general, nonsymmetric flow with the resolution of 64^3 modes. More recently, Brachet[15] reported results of simulations of the Taylor–Green flow performed with an effective resolution of up to 864^3 modes and Reynolds number $R_\lambda \approx 140$. A similar approach to increase range of scales and Reynolds numbers in numerical simulations of turbulence by employing symmetries of Navier–Stokes equations was pursued by Kida and his collaborators in a number of papers,[16–18] employing a flow with an even greater number of symmetries than the Taylor–Green vortex. At the present time these highly symmetric flows are the most computationally efficient means of numerically simulating isotropic turbulence with Reynolds number R_λ on the order 100.

Using the numerical code developed by Brachet[15] we have performed direct numerical simulations of the Taylor–Green vortex flow in order to generate a turbulent velocity field for the purpose of an analysis of the subgrid-scale nonlinear interactions. Since the details of such simulations were extensively described by Brachet *et al.*[14] and Brachet[15] we report here only a few main features of the time evolution of the flow and its properties at the end of the run. The velocity field at the end of the run is used in the subsequent sections for the analysis of the subgrid-scale interactions.

The flow is contained in a cube with a side length 2π resulting in wave numbers $\mathbf{k}=(k_1,k_2,k_3)$ in the spectral space with integer components k_i. In the physical space the flow is periodic with the period 2π in each coordinate direction x, y, and z. Because of the symmetries the flow never crosses the boundaries x, y, and $z=\pi$ and in the subsequent discussion it will be visualized in the so-called impermeable box[14] $0\leqslant x,y,z\leqslant\pi$. The effective spatial resolution in the simulations was 512^3 modes, which, after dealiasing by the 2/3 rule, provides the maximum wave number $k_m=170$ in each coordinate direction. Since the velocity and the length scale of the initial flow are order unity the large eddy turnover time is also order unity and the Reynolds number is equal to the inverse of molecular viscosity $1/\nu$ (3000 in the simulations). The simulations were run until maximum time $t_m=18$, i.e., for several large eddy turnover times, with the time step $\Delta t=0.0025$.

In Figs. 1(a)–1(d) we plot the time evolution of the total turbulent energy, the total dissipation rate ϵ, skewness S, and microscale Reynolds number R_λ, respectively. Until time $t\approx 5$ the evolution of the flow is essentially inviscid with the total energy nearly constant. During this period small scales are generated from the initial condition (1) resulting in a subsequent rapid rise of the dissipation rate which peaks at $t\approx 10$ and later decays because of the decrease in the intensity of turbulence caused by the viscous damping. The skewness, after fairly chaotic behavior until $t\approx 10$, at the end of the run approaches -0.5, which is the generally accepted value for this quantity in fully developed isotropic turbulence. The initial value of R_λ exceeds 1000, decays rapidly becoming an order of magnitude less at the time of the peak in the dissipation rate $t\approx 10$, and slowly approaches the final value $R_\lambda\approx 70$ at the end of the run.

It may be noted that previous simulations of this flow[14,15] were usually terminated shortly after the maximum in the dissipation rate had been reached, i.e., at $t\approx 10$. At that time turbulence is already well developed but values of some physical quantities like skewness may differ from values found in other direct numerical simulations of turbulence. These differences are often attributed to the symmetries of the Taylor–Green flow. However, simulations considered in this work, which were performed for longer times ($t_{\max}=18$), show that the skewness reaches its correct asymptotic value well after the peaking of the dissipation rate. Therefore some disagreements between the Taylor–Green flow results and other numerical simulations of nonsymmetric flows may be attributed to differences in the simulation times rather than to the effects of symmetries of the Taylor–Green flow.

The unnormalized energy and dissipation spectra at the end of the run are plotted in Fig. 2(a). A small number of modes in the low-wave-number shells causes relatively large fluctuations in these quantities at low wave numbers. In the range of wave numbers $k<20$ the energy spectrum conforms to the inertial $k^{-5/3}$ law with the Kolmogorov constant in the range 2.2–2.7. The dissipation spectrum peaks at $k\approx 20$ which, for the calculated Kolmogorov length scale $\eta=0.011$ in the units used, corresponds to $\eta k\approx 0.2$. This value agrees with experimental findings[19] locating the dissipation peak in high Reynolds number turbulence at a wave-number order of magnitude less than $1/\eta$. Because of a significant overlap of the energy containing range and the dissipation range it is unclear if the observed inertial range spectrum for $k<20$ is the result of the same dynamical processes that operate at very high Reynolds numbers where there exists a wide separation between the energy and the dissipation range. Also, an unusually high value of the Kolmogorov constant in the

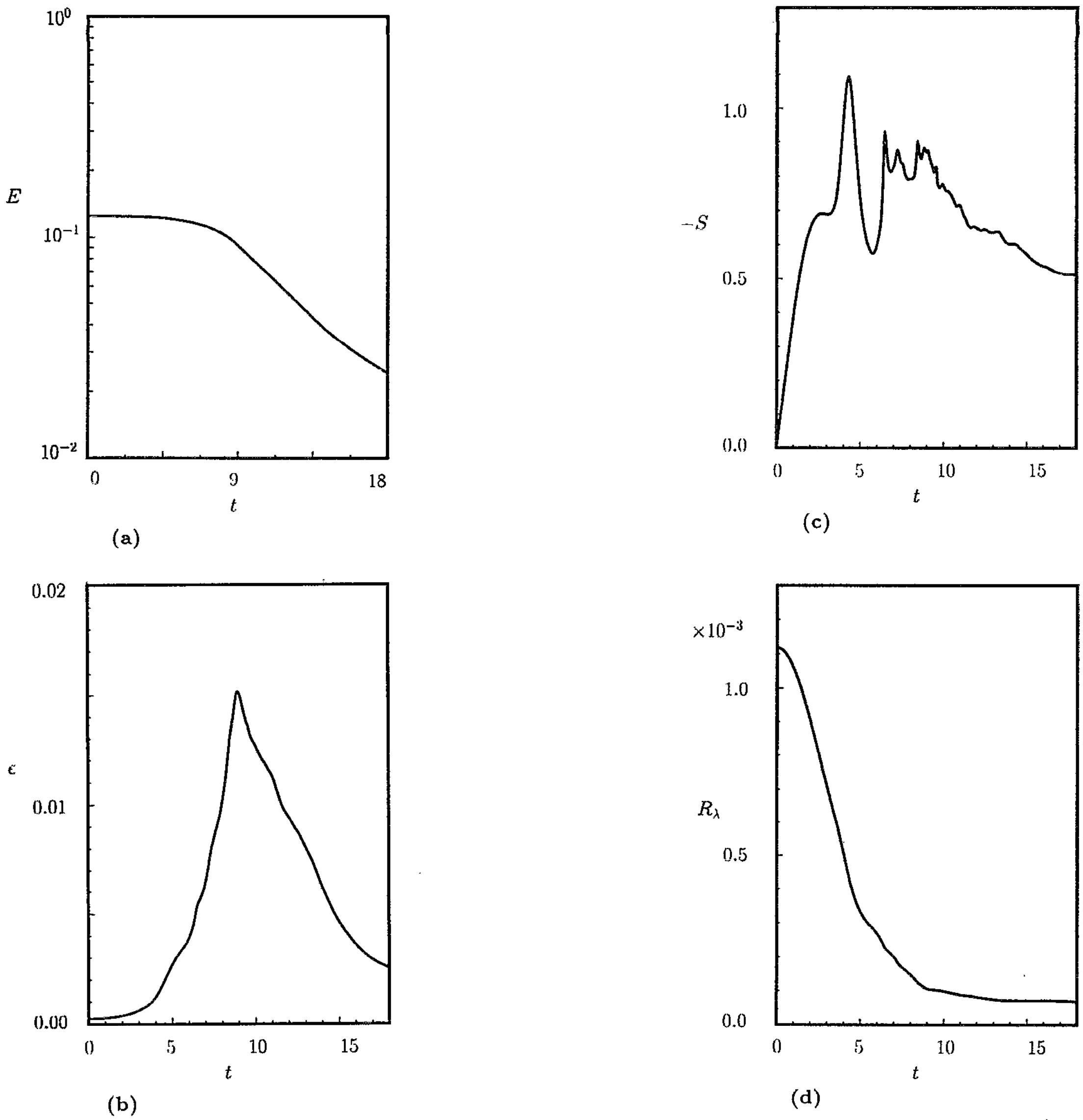

FIG. 1. Time evolution of flow quantities: (a) total kinetic energy; (b) total dissipation; (c) skewness; (d) microscale Reynolds number.

simulations casts doubt on the significance of the observed inertial subrange as being indicative of high Reynolds number turbulence dynamics. We may claim at best that the Reynolds number in the simulations is high enough to capture the beginnings of the inertial range dynamics but too low to separate it from the effects of the dissipation range dynamics. In the far dissipation range for $k>20$ the dissipation and the nonlinear transfer spectra balance each other and have the functional form proportional to $k^{-2}\exp(-ak)$ as seen in Fig. 2(b). This form was derived by Domaradzki[20] using scaling properties of the detailed energy transfer observed in low Reynolds number turbulence.

III. BASIC QUANTITIES

For homogeneous turbulence incompressible Navier–Stokes equations in spectral (Fourier) representation are

$$\frac{\partial}{\partial t} u_n(\mathbf{k}) = -\nu k^2 u_n(\mathbf{k}) + N_n(\mathbf{k}). \tag{2}$$

Here, $u_n(\mathbf{k})$ is the velocity field in spectral space, with the explicit dependence on time omitted, ν is the kinematic viscosity, and $N_n(\mathbf{k})$ is the nonlinear term

$$N_n(\mathbf{k}) = -\frac{i}{2} P_{nlm}(\mathbf{k}) \int d^3p\, u_l(\mathbf{p}) u_m(\mathbf{k}-\mathbf{p}), \tag{3}$$

where tensor $P_{nlm}(\mathbf{k})$ accounts for the pressure and incompressibility effects. The summation convention is assumed throughout.

Let us assume that the wave-number space is divided into two nonoverlapping regions, $\mathscr{L}$ ($|\mathbf{k}|<k_c$) signifying large scales, and $\mathscr{S}$ ($|\mathbf{k}|>k_c$) signifying small scales. In the LES terminology these scales are also referred to as the resolved and unresolved scales, respectively. In the LES an evolution equation for the velocity field $u_n(\mathbf{k})$ truncated to the region $\mathscr{L}$

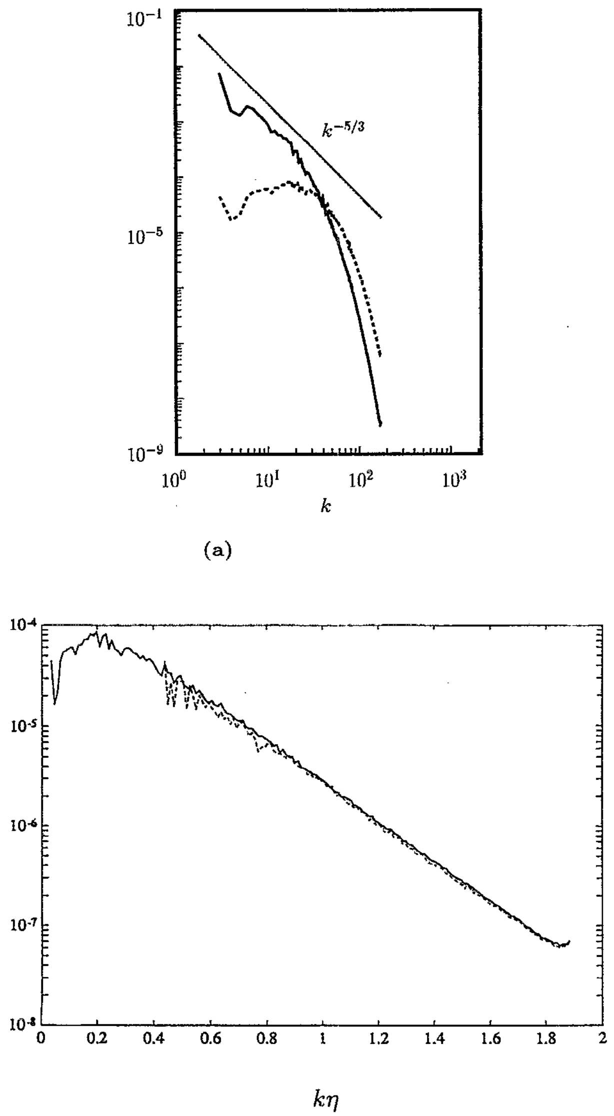

(b)

FIG. 2. Spectral quantities at the end of the run ($t=18$): (a) unnormalized spectra of the energy (solid line) and the dissipation (broken line); (b) the dissipation spectrum (solid line) and the transfer spectrum (broken line) outside the energy containing range. Both quantities plotted using a log-linear scale to accentuate their exponential behavior.

$$u_n^{\mathscr{L}}(\mathbf{k})=\begin{cases}u_n(\mathbf{k}), & \text{if } \mathbf{k}\in\mathscr{L},\\ 0, & \text{otherwise,}\end{cases} \tag{4}$$

is sought. The truncation operation is trivially applied to the linear terms in Eq. (2). The nonlinear term (3) is decomposed as follows. First, it is computed with one of the contributing velocity fields truncated to $\mathscr{U}$ and the other to $\mathscr{V}$, where $\mathscr{U}$ and $\mathscr{V}$ may be any of the two previously prescribed regions. Details of such calculations are provided by Domaradzki and Rogallo.[21,22] The resulting quantity, denoted by $N_n^{\mathscr{U}\mathscr{V}}(\mathbf{k})$, describes the modification of the mode $\mathbf{k}$ caused by all triad interactions involving $\mathbf{k}$ and two other scales, one belonging to $\mathscr{U}$ and the other to $\mathscr{V}$. Second, to retain the effect of such nonlinear interactions on the large scales only, the quantity $N_n^{\mathscr{U}\mathscr{V}}(\mathbf{k})$ is truncated to the region $\mathscr{L}$, with the result denoted by $N_n^{\mathscr{L}\mathscr{U}\mathscr{V}}(\mathbf{k})$. The evolution equation for the large scales $\mathscr{L}$ becomes

$$\frac{\partial}{\partial t} u_n^{\mathscr{L}}(\mathbf{k})=-\nu k^2 u_n^{\mathscr{L}}(\mathbf{k})+N_n(\mathbf{k}\,|\,k_c)+N_n^s(\mathbf{k}\,|\,k_c), \tag{5}$$

where the resolved nonlinear term is

$$N_n(\mathbf{k}\,|\,k_c)=N_n^{\mathscr{L}\mathscr{L}\mathscr{L}}(\mathbf{k}), \tag{6}$$

and the subgrid-scale nonlinear term $N_n^s(\mathbf{k}\,|\,k_c)$ is

$$N_n^s(\mathbf{k}\,|\,k_c)=N_n^{\mathscr{L}\mathscr{L}\mathscr{S}}(\mathbf{k})+N_n^{\mathscr{L}\mathscr{S}\mathscr{S}}(\mathbf{k}). \tag{7}$$

In practice, the most straightforward way to compute (6) and (7) is to first use (3) with the full velocity fields $u_l(\mathbf{p})$ and $u_m(\mathbf{k}-\mathbf{p})$ and truncate the result to the region $\mathscr{L}$ to obtain the total nonlinear term

$$N_n^{\text{tot}}(\mathbf{k}\,|\,k_c)=N_n(\mathbf{k}\,|\,k_c)+N_n^s(\mathbf{k}\,|\,k_c). \tag{8}$$

Next, Eq. (3) is used again with the truncated velocity fields $u_l^{\mathscr{L}}(\mathbf{p})$ and $u_m^{\mathscr{L}}(\mathbf{k}-\mathbf{p})$ and the result is truncated to the region $\mathscr{L}$ giving the resolved nonlinear term $N_n(\mathbf{k}\,|\,k_c)$ [Eq. (6)]. The subgrid-scale nonlinear term (7) is obtained as the difference between the total nonlinear term (8) and the resolved nonlinear term (6).

The above-described procedure has its exact counterpart in the physical space representation. An inverse Fourier transform, signified by a tilde, of $N_n(\mathbf{k})$ [Eq. (3)] is the sum of the convective and pressure terms in the Navier–Stokes equation in the physical space coordinates

$$\widetilde{N}_n(\mathbf{x})=-\widetilde{u}_i(\mathbf{x})\,\frac{\partial \widetilde{u}_n(\mathbf{x})}{\partial x_i}-\frac{\partial p(\mathbf{x})}{\partial x_n}. \tag{9}$$

Similarly, using $N_n^{\mathscr{U}\mathscr{V}}(\mathbf{k})$ we can define its physical space counterpart $\widetilde{N}_n^{\mathscr{U}\mathscr{V}}(\mathbf{x})$ as well as $\widetilde{N}_n^{\mathscr{K}\mathscr{U}\mathscr{V}}(\mathbf{x})$ which is the inverse Fourier transform of $N_n^{\mathscr{U}\mathscr{V}}(\mathbf{k})$ truncated to the region $\mathscr{K}$ (which is either $\mathscr{L}$ or $\mathscr{S}$). Here $\widetilde{N}_n^{\mathscr{U}\mathscr{V}}(\mathbf{x})$ can be interpreted as the contribution to the rate of change of the velocity field $\widetilde{u}_n(\mathbf{x})$ at a point $\mathbf{x}$ made by the nonlinear interactions involving modes from the spectral regions $\mathscr{U}$ and $\mathscr{V}$. Note that these interactions influence all modes $\mathbf{k}$ which can form a triangle with two other modes such that one is in $\mathscr{U}$ and the other in $\mathscr{V}$. Also, $\widetilde{N}_n^{\mathscr{K}\mathscr{U}\mathscr{V}}(\mathbf{x})$ represents a contribution to the rate of change of $\widetilde{u}_n(\mathbf{x})$ which is made by all modes from $\mathscr{K}$ interacting nonlinearly with modes in $\mathscr{U}$ and $\mathscr{V}$. Finally, the inverse Fourier transform of (5) is

$$\frac{\partial}{\partial t}\widetilde{u}_n^{\mathscr{L}}(\mathbf{x})=\nu\nabla^2\widetilde{u}_n^{\mathscr{L}}(\mathbf{x})+\widetilde{N}_n(\mathbf{x}\,|\,k_c)+\widetilde{N}_n^s(\mathbf{x}\,|\,k_c), \tag{10}$$

where the resolved nonlinear term $\widetilde{N}_n(\mathbf{x}\,|\,k_c)$ and the subgrid-scale term $\widetilde{N}_n^s(\mathbf{x}\,|\,k_c)$ in the physical space are obtained Fourier transforming (6) and (7), respectively.

In the LES the most fundamental requirement is that the models employed properly approximate effects of subgrid-scale interactions on the energetics of the resolved scales. Thus, in assessing the models, energy equations rather than momentum equations are usually considered.

In the spectral space the equation for the energy amplitude $\frac{1}{2}|u(\mathbf{k})|^2 = \frac{1}{2}u_n(\mathbf{k})u_n^*(\mathbf{k})$ of mode $\mathbf{k}$ obtained from (2) is

$$\frac{\partial}{\partial t}\frac{1}{2}|u(\mathbf{k})|^2 = -2\nu k^2 \frac{1}{2}|u(\mathbf{k})|^2 + T(\mathbf{k}), \tag{11}$$

where $T(\mathbf{k})$ is the nonlinear energy transfer

$$T(\mathbf{k}) = \mathrm{Re}[u_n^*(\mathbf{k})N_n(\mathbf{k})]. \tag{12}$$

For homogeneous turbulence the above equations are usually considered after summing up contributions from all modes with a prescribed wavelength $|\mathbf{k}| = k$, giving

$$\frac{\partial}{\partial t}E(k) = -2\nu k^2 E(k) + T(k), \tag{13}$$

where $E(k)$ and $T(k)$ are the classical energy and transfer spectra, respectively, for homogeneous turbulence.

Similarly, the detailed energy transfer to/from mode $\mathbf{k}$ caused by its interactions with wave numbers $\mathbf{p}$ in a prescribed region $\mathscr{P}$ of the wave-number space and $\mathbf{q} = \mathbf{k} - \mathbf{p}$ in another region $\mathscr{Q}$ is

$$T^{\mathscr{P}\mathscr{Q}}(\mathbf{k}) = \mathrm{Re}[u_n^*(\mathbf{k})N_n^{\mathscr{P}\mathscr{Q}}(\mathbf{k})]. \tag{14}$$

Truncating $T^{\mathscr{P}\mathscr{Q}}(\mathbf{k})$ to another region $\mathscr{K}$ results in the quantity $T^{\mathscr{K}\mathscr{P}\mathscr{Q}}(\mathbf{k})$ which is interpreted as the energy transfer to the region $\mathscr{K}$ resulting from nonlinear interactions of scales in $\mathscr{K}$ with scales in $\mathscr{P}$ and $\mathscr{Q}$. For homogeneous turbulence the regions $\mathscr{P}$ and $\mathscr{Q}$ are usually chosen as spherical wave-number bands centered at wave numbers p and q, respectively. In this case quantity $T^{\mathscr{P}\mathscr{Q}}(\mathbf{k})$ will be denoted by $T(\mathbf{k}|p,q)$. Summing quantity $T(\mathbf{k}|p,q)$ over spherical shells with thickness $\Delta k = 1$ centered at wave number k gives a function denoted by either $T^{\mathscr{K}\mathscr{P}\mathscr{Q}}(k)$ or $T(k|p,q)$

$$T^{\mathscr{K}\mathscr{P}\mathscr{Q}}(k) = T(k|p,q) = \sum_{k-(1/2)\Delta k < |\mathbf{k}| < k+(1/2)\Delta k} T(\mathbf{k}|p,q). \tag{15}$$

Total nonlinear energy transfer $T(k)$ to the wave-number band k is obtained by summing contributions $T(k|p,q)$ from all possible bands p and q:

$$T(k) = \sum_p \sum_q T(k|p,q) = \sum_p P(k|p). \tag{16}$$

Here, the function $P(k|p)$ is a result of summation of $T(k|p,q)$ over all q bands and is interpreted as the energy transfer between wave-number bands k and p.

With this notation, the energy equation for the energy spectrum $E^{\mathscr{L}}(k)$ of resolved scales, obtained from Eq. (5), is

$$\frac{\partial}{\partial t}E^{\mathscr{L}}(k) = -2\nu k^2 E^{\mathscr{L}}(k) + T(k|k_c) + T^s(k|k_c), \tag{17}$$

where

$$T(k|k_c) = T^{\mathscr{L}\mathscr{L}\mathscr{L}}(k) \tag{18}$$

and

$$T^s(k|k_c) = T^{\mathscr{L}\mathscr{L}\mathscr{S}}(k) + T^{\mathscr{L}\mathscr{S}\mathscr{S}}(k). \tag{19}$$

Equivalent expressions in the physical space are obtained by considering an equation for the rate of change of the turbulent energy of the resolved scales $e^{\mathscr{L}}(\mathbf{x}) = \frac{1}{2}\tilde{u}_n^{\mathscr{L}}(\mathbf{x})\tilde{u}_n^{\mathscr{L}}(\mathbf{x})$:

$$\frac{\partial e^{\mathscr{L}}(\mathbf{x})}{\partial t} = \nu\tilde{u}_n^{\mathscr{L}}(\mathbf{x})\nabla^2\tilde{u}_n^{\mathscr{L}}(\mathbf{x}) + \tilde{T}(\mathbf{x}|k_c) + \tilde{T}^s(\mathbf{x}|k_c), \tag{20}$$

where

$$\tilde{T}(\mathbf{x}|k_c) = \tilde{u}_n^{\mathscr{L}}(\mathbf{x})\tilde{N}_n(\mathbf{x}|k_c), \tag{21}$$

is the resolved energy transfer and

$$\tilde{T}^s(\mathbf{x}|k_c) = \tilde{u}_n^{\mathscr{L}}(\mathbf{x})\tilde{N}_n^s(\mathbf{x}|k_c) \tag{22}$$

is the subgrid-scale energy transfer in the physical space representation. This last expression (22) accounts for all physical processes involving nonlinear interactions between the resolved scales and the unresolved subgrid scales. In a traditional approach to deriving LES equations through spatial filtering of Navier–Stokes equations this term is often represented by a sum of a redistribution term with the vanishing global mean and a subgrid-scale dissipation term with a nonzero mean. In assessing LES models using direct numerical simulations databases usually only SGS dissipation is considered.[23] In those investigations the SGS dissipation is often averaged either over an entire computational domain or over subdomains, e.g., over horizontal planes in a channel flow, in order to evaluate global energy flux to the subgrid scales. However, in LES the redistribution subgrid-scale term is also unknown and in principle both terms are needed to fully account for the effect of the subgrid-scale interactions in the physical space representation if no averaging is performed. For this reason in this work we consider quantity (22) rather than more traditional SGS dissipation.

IV. RESULTS

Using the methodology described in the previous section and employing the numerically simulated velocity fields it is possible to compute directly the subgrid-scale energy transfer for any prescribed cutoff wave number $k_c < k_m$. It is customary to represent spectral subgrid-scale energy transfer in terms of the subgrid-scale eddy viscosity

$$\nu_e(k|k_c) = -\frac{T^s(k|k_c)}{2k^2E^{\mathscr{L}}(k)}, \quad k < k_c, \tag{23}$$

which, following Kraichnan,[4] is usually normalized by the factor equal to the product of the velocity scale $[E(k_c)k_c]^{1/2}$ and the length scale $1/k_c$ at the cutoff k_c,

$$\nu_e^K(k|k_c) = \frac{\nu_e(k|k_c)}{[E(k_c)/k_c]^{1/2}} \tag{24}$$

This procedure to compute the spectral eddy viscosity was previously employed by Domaradzki *et al.*[11] who used data from a direct numerical simulation of isotropic turbulence

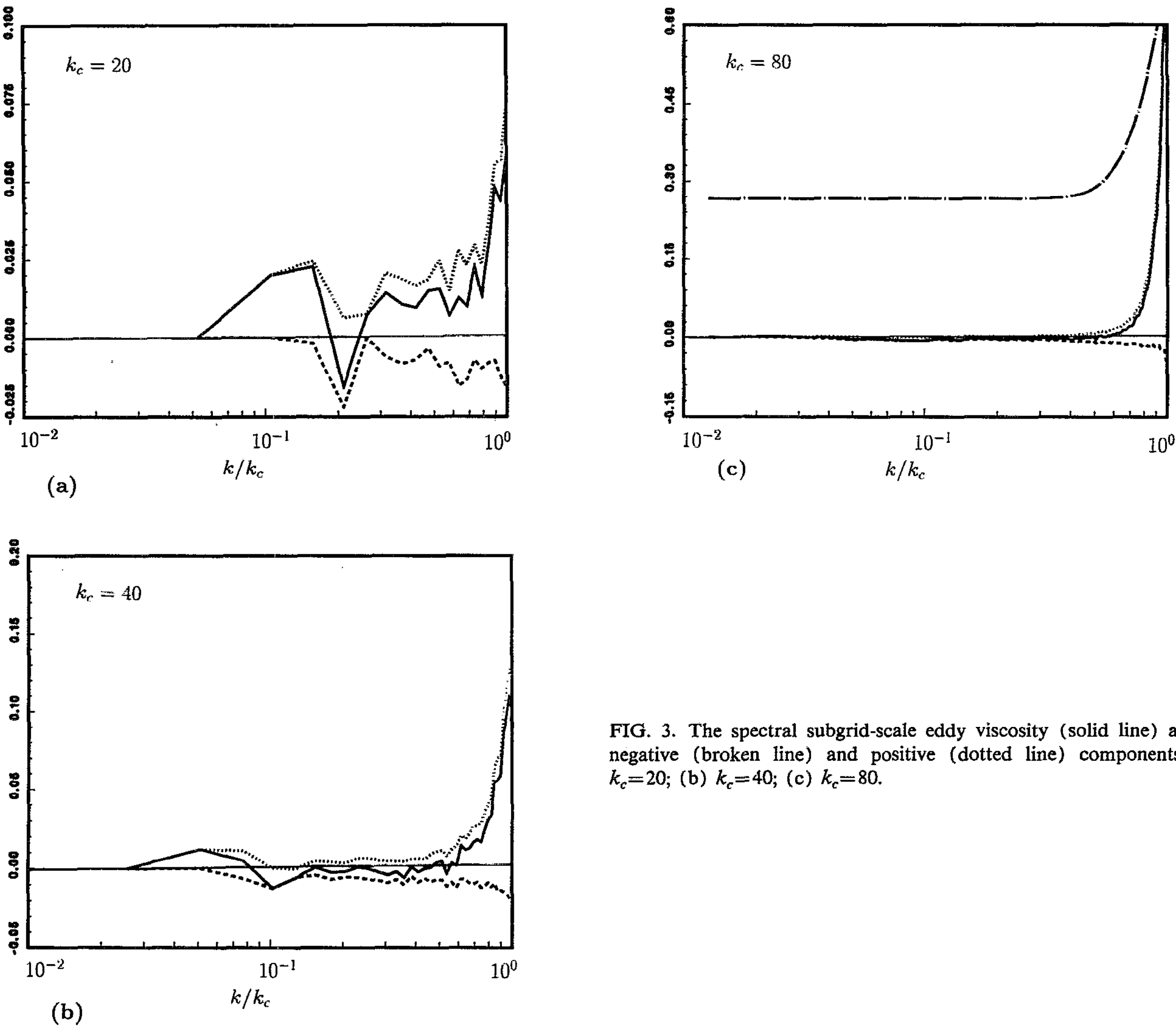

FIG. 3. The spectral subgrid-scale eddy viscosity (solid line) and its negative (broken line) and positive (dotted line) components: (a) k_c=20; (b) k_c=40; (c) k_c=80.

and by Lesieur and Rogallo[24] and Chasnov[8] who used data from a large eddy simulation of isotropic turbulence.

In order to compute the function $T^s(k|k_c)$, which depends on the length of the wave number k, according to Eq. (15) summation over all wave vectors **k** in a thin spherical shell centered at k must be performed. The components of such a sum are in general of both signs implying that a particular mode **k** may be either losing energy (forward transfer) or gaining energy (inverse transfer) because of the subgrid-scale nonlinear interactions. To assess the relative importance of these two processes we have performed partial summations over components of the same sign, effectively splitting the subgrid-scale energy transfer to/from scales k into the forward and the inverse transfer contributions. This procedure is equivalent to decomposing the total eddy viscosity into two parts, a positive one associated with the forward energy transfer, and a negative one associated with the inverse energy transfer. Such a decomposition is a straightforward extension of the original procedure[11] used in the above-mentioned works but provides more detailed information about the subgrid-scale energy transfer process not available in those papers.

In Fig. 3 we plot the total eddy viscosity and its positive and negative components computed for three different cutoff wave numbers: one, $k_c=20$, at the end of the (nominal) inertial subrange; the next, $k_c=40$, at the beginning of the dissipation range; and the last one, $k_c=80$, deep in the dissipation range. For $k_c=20$ the total eddy viscosity is predominantly positive, with the absolute values of the negative component about 30%–50% of the values of the positive component for $k/k_c<0.6$. For $k/k_c>0.6$ the ratio of the negative to the positive component decreases to about 20%. For $k_c=40$ in the range $k/k_c<0.6$ the positive and negative components nearly balance each other with the resulting total eddy viscosity close to zero. For $k/k_c>0.6$ both components exhibit cusplike behavior with the cusp for the positive component much stronger than for the negative one. Nevertheless, even close to the cutoff the ratio of the negative to the positive component is about 15%. For the case $k_c=80$ in the range $k/k_c<0.6$ the positive component is practically zero and the negative one is slightly less than zero, resulting in small negative values of the total eddy viscosity. Beyond that range, for k approaching the cutoff, the positive component increases very rapidly, reaching at the cutoff k_c values a factor 20 greater than the values of the negative component. In Fig. 3(c) we

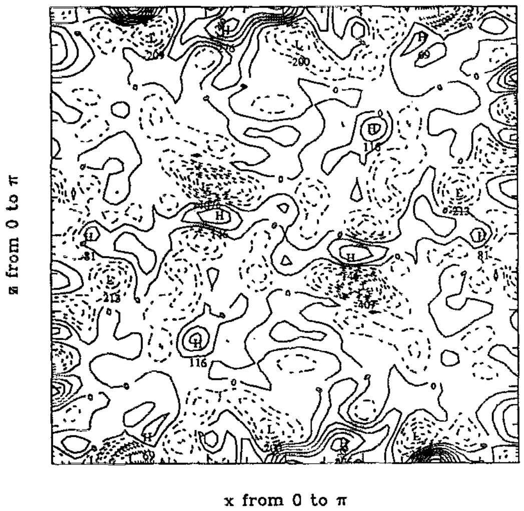

(a)

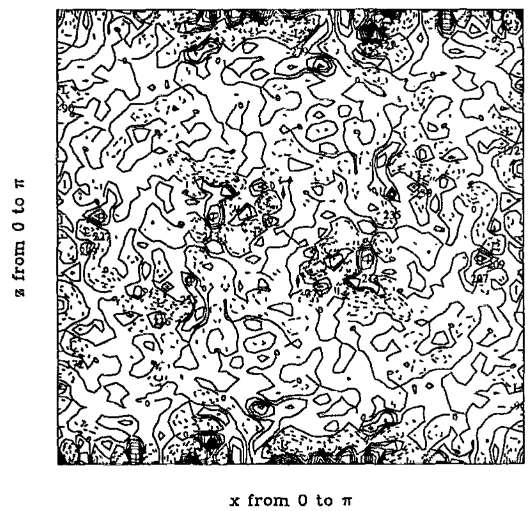

(b)

FIG. 4. The subgrid-scale energy transfer in the physical space representation: (a) $k_c=20$; (b) $k_c=40$. Plane $y=\pi/4$ in the impermeable box is shown. Here and in all subsequent contour plots the solid lines represent positive values and the broken lines represent negative values.

also plot the subgrid-scale eddy viscosity calculated by Kraichnan[4] and Cholet and Lesieur[5] from the analytical theories of turbulence under the assumption of the infinite inertial range. This function is essentially constant (equal to 0.267) for $k/k_c<0.6$, and exhibits the cusplike behavior for $k/k_c>0.6$. We conclude from this analysis that the spectral inverse energy transfer may be quite significant, in some cases comparable to the forward transfer for given scales k. However, in all cases the forward transfer dominates as the cutoff wave number is approached. Since the transfer is obtained by multiplying the eddy viscosity by k^2, the cusp in the eddy viscosity for $k/k_c>0.6$ is actually even more significant for the subgrid-scale transfer.

Using Eq. (22) we have computed the subgrid-scale energy transfer in the physical space $\widetilde{T}^s(\mathbf{x}|k_c)$ for several spectral cutoff wave numbers. In Fig. 4 we plot a cross section of this quantity for $k_c=20$ and 40 for a plane in the impermeable box located at $y=\pi/4$. The larger spectral cutoff wave number results in the presence of smaller scales in the physical space. Regions of the forward transfer (broken contours) and the inverse transfer (solid contours) are clearly visible. For both cutoff wave numbers we have computed volume-averaged forward and inverse transfer normalized by their sum, i.e., by the total subgrid scale energy transfer (a negative quantity). For $k_c=20$ the normalized inverse transfer is -1.06 and the forward transfer is 2.06 while for the cutoff $k_c=40$ the same quantities are -2.83 and 3.83, respectively. Thus the absolute value of the ratio of the inverse transfer to the total subgrid-scale transfer increases from about 1 to about 3 for increasing cutoff wave number (i.e., decreasing filter width in the spatial averaging procedure). This trend is consistent with the results of Piomelli *et al.*[23] obtained for compressible isotropic turbulence. For the largest filter width used in their work the magnitude of the inverse transfer is comparable to the total subgrid-scale transfer, with the ratio of these two quantities increasing for decreasing filter width.

Even though the overall subgrid-scale transfer integrated over the computational box is negative, the forward and inverse transfer regions in these plots are roughly in balance, again in agreement with the results of Piomelli *et al.*[23] who found that about 50% of all points in a computational domain were characterized by the inverse energy transfer. This indicates that both effects may be equally important in the dynamics of the flow. This conclusion agrees with the corresponding conclusion reached in the analysis of the spectral subgrid-scale transfer. It should be noted, however, that there is no direct relation between sets of spectral modes characterized by positive/negative transfer and the physical space regions with the same characteristics.

Assuming that in the large-scale momentum equation (5) the subgrid-scale nonlinear term $N_n^s(\mathbf{k}|k_c)$ is represented using the classical spectral eddy viscosity model $\nu_e(k|k_c)$ of Kraichnan[4] and Cholet and Lesieur[5]

$$N_n^s(\mathbf{k}|k_c) = -\nu_e(k|k_c)k^2 u_n^{\mathscr{L}}(\mathbf{k}), \tag{25}$$

we have calculated the physical space subgrid-scale energy transfer for this model from (22). The results of the calculations are plotted in Fig. 5 for $k_c=20$ and the same cross-plane as in Fig. 4. The modeled transfer is predominantly of the forward type as expected from the use of the strictly positive eddy viscosity but the appearance of weak inverse transfer regions may seem surprising. However, it should be noted that the molecular viscosity term in the incompressible Navier–Stokes equations results in two distinct effects in the energy equation: the kinetic energy dissipation, which is negative everywhere, and the change in the kinetic energy caused by work done by viscous stresses, which locally in space may be either positive or negative. Therefore any model which approximates the subgrid-scale nonlinear term N_n^s by a viscouslike term in the Navier–Stokes equations may contain regions of the increasing ki-

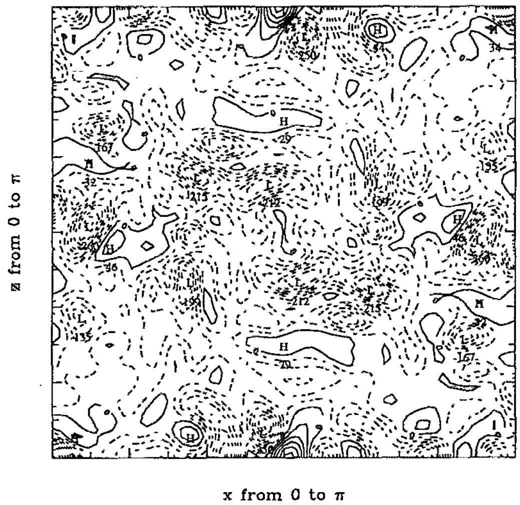

FIG. 5. The subgrid-scale energy transfer in the physical space computed using the spectral eddy viscosity model of Kraichnan[4] and Chollet and Lesieur.[5]

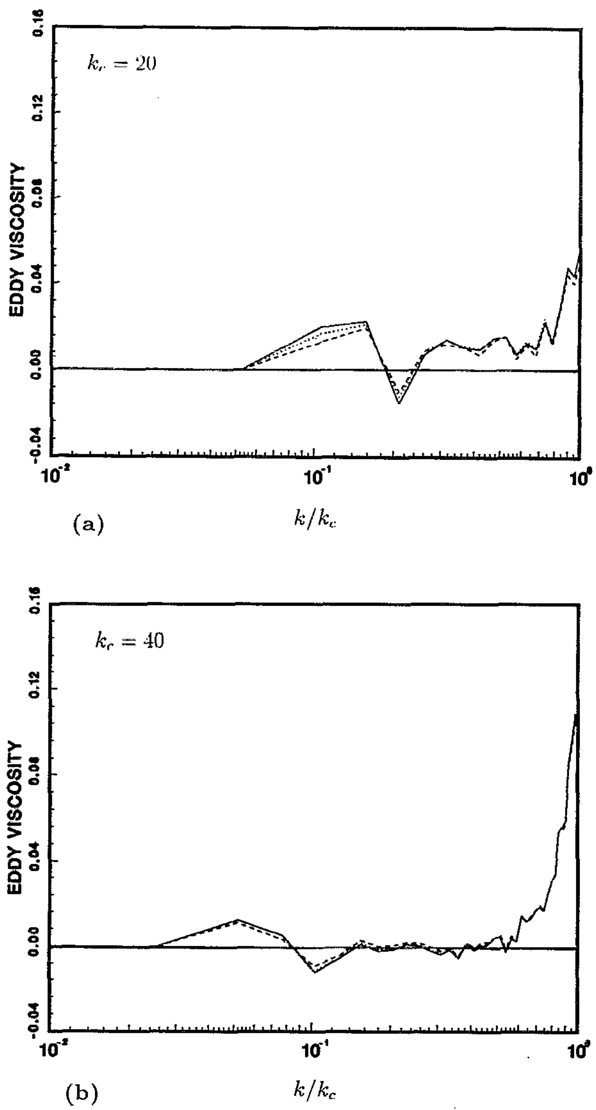

FIG. 6. The spectral subgrid-scale eddy viscosity: (a) $k_c=20$; (b) $k_c=40$. The velocity fields used to compute this quantity were the full field (solid line), the full field truncated at $(3/2)k_c$ (broken line), and the full field truncated at $2k_c$ (dotted line).

netic energy caused by work done by the modeled stresses. In practice, however, as seen in Fig. 5, these positive regions are quite insignificant since they occupy much less space than the negative regions and also have much lower maximum values. Obviously, such models give a poor representation of the actual subgrid-scale energy transfer as seen by comparing the actual and modeled transfers shown in Figs. 4(a) and 5, respectively. The conclusions from the physical space analysis of the subgrid-scale energy transfer parallel those drawn from the spectral space analysis: the relative importance of the inverse energy transfer process and an inability of the classical subgrid-scale models to properly account for it.

Cusps observed in spectral eddy viscosities in the vicinity of the cutoff wave number suggest that the total energy transfer across this wave number is dominated by energy exchanges among resolved and unresolved scales from the vicinity of the cutoff. Indeed, it has been established in a number of papers[18,21,22,25] that in numerically simulated turbulence at low Reynolds numbers the energy transfer beyond the energy containing range is local, occurring between scales of similar size, even though the nonlocal wave-number triads with one scale in the energy containing range are responsible for this local transfer. One would thus expect that the subgrid-scale nonlinear interactions between the resolved scales ($k<k_c$) and the unresolved scales characterized by wave numbers slightly greater than the cutoff wave number k_c will dominate the subgrid-scale energy transfer process. To evaluate this hypothesis in more detail we have calculated, for several values of the cutoff wave number k_c, the subgrid-scale energy transfer for the truncated velocity fields obtained from the original field by setting to zero all modes with wave numbers $k>ck_c$, where c was equal to 3/2 and 2. In this way the effect of all modes $k>ck_c$ on the subgrid-scale energy transfer is eliminated. In Fig. 6 we plot the resulting spectral subgrid-scale eddy viscosities (24) for $k_c=20$ and 40 and compare them with the eddy viscosities computed using the full velocity field, i.e., with all modes $k<k_m$ being nonzero. It is seen that the value of the eddy viscosity computed for $c=3/2$ provides a very good approximation to the total eddy viscosity while for $c=2$ both quantities are practically indistinguishable on the plots. The similarly calculated subgrid-scale transfer in the physical space (22) is shown in Fig. 7 for the cutoff wave number $k_c=20$ and two values of the parameter c, 3/2 and 2. The plane shown is the same as in Fig. 4. The spatial structure of the subgrid-scale energy transfer in Figs. 7 and 4(a) is the same, with differences seen only in the values of the transfer at particular locations. For $c=3/2$ the peak values of the approximated transfer [Fig. 7(a)] may depart by about 10% from the exact values [Fig. 4(a)] with the departures decreasing to about 5% for $c=2$ [Fig. 7(b)]. Therefore, both in the spectral and the physical space representation the subgrid-scale energy transfer for the resolved modes

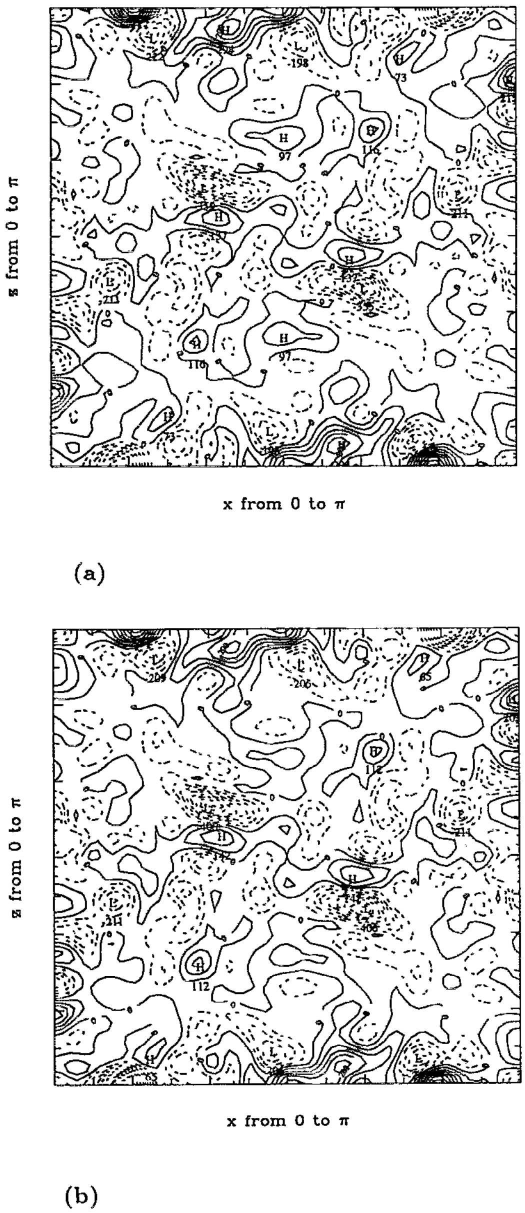

FIG. 7. The physical space subgrid-scale energy transfer computed for $k_c=20$ and the full fields truncated at (a) $(3/2)k_c$ and (b) $2k_c$.

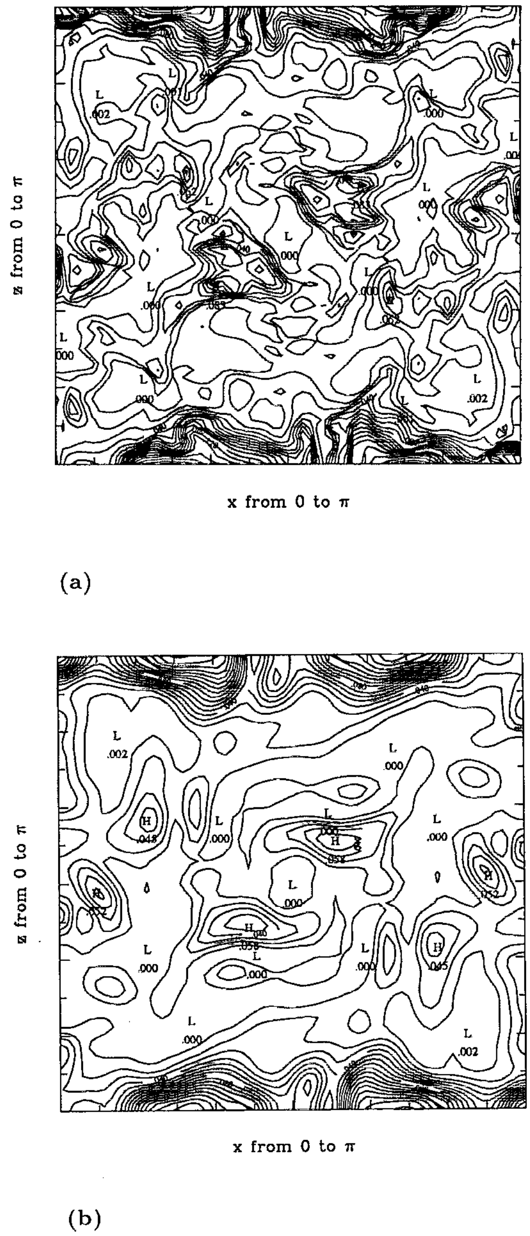

FIG. 8. The kinetic energy field in a plane $y=(3/4)\pi$ in the impermeable box: (a) computed using the full velocity field; (b) computed using the resolved velocity field with the truncation wave number $k_c=20$.

$k<k_c$ can be determined with high accuracy by considering their interactions with a limited range of unresolved modes $k_c<k\leqslant 2k_c$. It may be instructive to note that for $k_c=20$ and $k_m=170$ the resolved modes constitute about 0.0016 of all modes, and modes with $k\leqslant 2k_c$ about 0.013 of all modes. Thus the dynamics of the largest 0.16% modes is determined almost entirely by their nonlinear interactions with about 1% of all modes, the remaining 99% of the modes not affecting visibly the largest scales. Moreover, the lack of direct influence of small scales $k>2k_c$ on the energetics of the large resolved scales $k<k_c$ implies that the direct nonlocal energy transfer, inherent in the classical eddy viscosity theories,[19] is not present in our simulations. The dynamics of the largest modes observed in the simulations is quite similar to the classical picture of the dynamics of the energy containing range in high Reynolds number turbulence. Quoting Batchelor:[26] "It seems that the energy-containing eddies determine the rate of energy transfer by their mutual interactions, and the larger wavenumbers adjust themselves, according to the Reynolds number, in order to convert this energy into heat at the required rate."

For the purpose of subgrid-scale modeling it is important to investigate relations between observed subgrid-scale energy transfer and various features of the resolved velocity field (4). In Figs. 8, 9, and 10 we plot in the physical space representation the kinetic energy $\frac{1}{2}\mathbf{u}(\mathbf{x})\cdot\mathbf{u}(\mathbf{x})$, the enstrophy $\frac{1}{2}\omega(\mathbf{x})\cdot\omega(\mathbf{x})$, where $\omega(\mathbf{x})$ is the vorticity, and the dissipation rate $\frac{1}{2}\nu(\partial u_i/\partial x_k+\partial u_k/\partial x_i)^2$, respectively. All these quantities are computed using both the full velocity field (all modes $k<k_m$ are nonzero) and the velocity field (4) truncated at $k_c=20$. One cross-sectional plane at

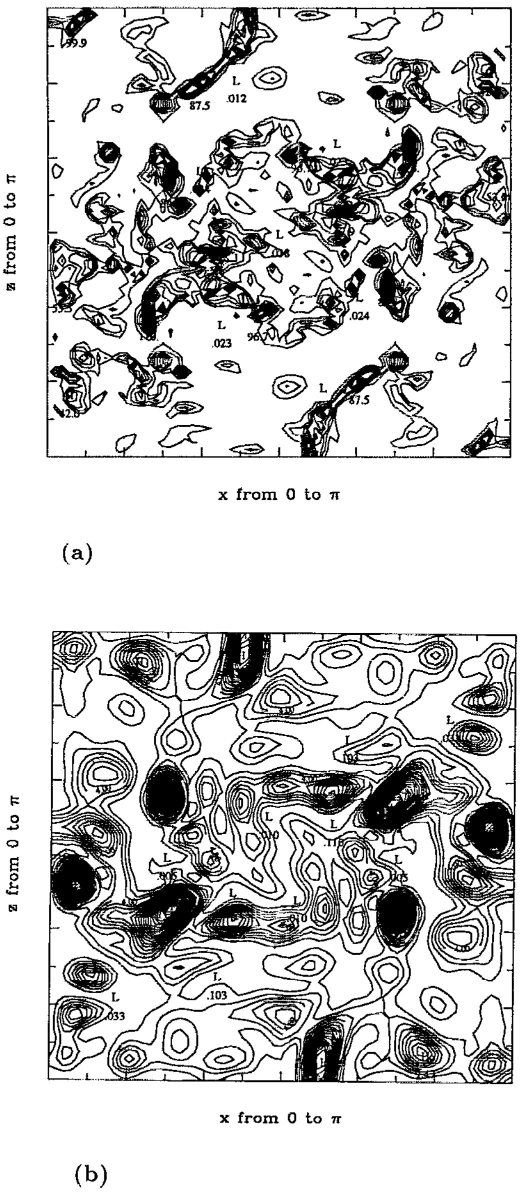

FIG. 9. The enstrophy field in a plane $y=(3/4)\pi$ in the impermeable box: (a) computed using the full velocity field; (b) computed using the resolved velocity field with the truncation wave number $k_c=20$.

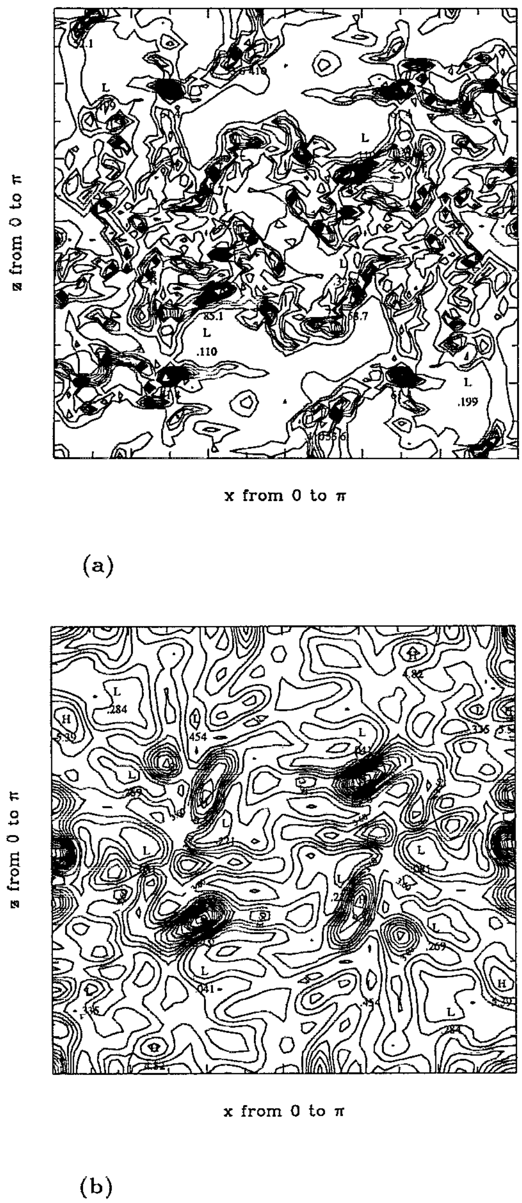

FIG. 10. The dissipation field in a plane $y=(3/4)\pi$ in the impermeable box: (a) computed using the full velocity field; (b) computed using the resolved velocity field with the truncation wave number $k_c=20$.

the location $y=(3/4)\pi$ in the impermeable box is plotted and for comparison we also plot in Fig. 11 the subgrid-scale energy transfer in the same plane. The spatial structure of energy fields for the full and truncated fields is nearly the same. This feature is expected since the modes $k<k_c$ contain most of the total energy. The peak values of the energy for the full field may exceed by 30% the peak values for the truncated field. The maximum values for the dissipation and the enstrophy fields computed using the full velocity fields are greater by a factor of 5 than for the truncated fields, indicating fairly large contributions coming from higher wave numbers $k>k_c$. The importance of these wave numbers is also reflected in the spatial structure of these quantities, with the full fields showing the presence of much smaller scales than the truncated fields. Despite these differences between the full and the truncated fields, for the enstrophy the spatial structure of the large-scale component [Fig. 9(b)] is remarkably similar to the structure of the total enstrophy [Fig. 9(a)]. In particular the regions of large values of the total enstrophy are very well correlated with the regions where the truncated field also gives large values. This result is somewhat surprising since the large-scale enstrophy field is determined using only 0.16% of all modes. It suggests that these largest scales contain most of phase information required to determine spatial structure of the enstrophy field, and the role of higher wave-number modes is to merely reflect the fact that the velocity gradients are steeper than can be resolved

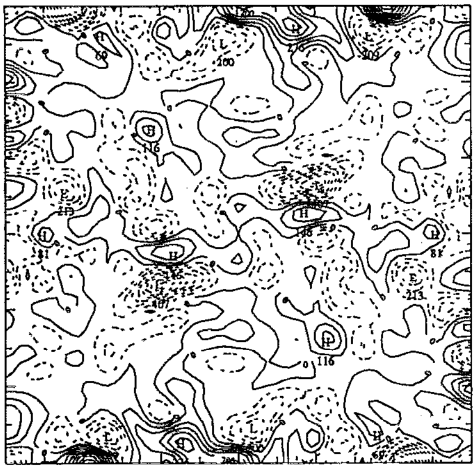

FIG. 11. The subgrid-scale energy transfer in the physical space representation computed for the cutoff wave number $k_c=20$ and shown in a plane $y=(3/4)\pi$ in the impermeable box.

by the low-wave-number modes. In other words, larger wave numbers in the spectral space are needed to resolve steep velocity gradients rather than small eddies thought of as small, individual flow structures like localized vortices. The level of correlation between the full and truncated fields for the dissipation is lower. The regions of the most intense dissipation for the truncated field [located along diagonals, halfway between the center and the corners of the plotted plane in Fig. 10(b)] correlate well with the full dissipation field in the same region [Fig. 10(a)] but some equally strong regions in the full field farther away from the center do not have clear counterparts in the truncated field. Finally, all three quantities computed using the truncated velocity field were compared with the subgrid-scale energy transfer plotted in Fig. 11. There is some level of spatial correlation between the subgrid-scale transfer and the enstrophy and the dissipation fields, with the regions of significant transfer in the vicinity (but not on the top of) regions of large enstrophy and dissipation. Also, the regions of intense large-scale dissipation are usually located on the peripheries of the regions of intense large-scale enstrophy. Interestingly, the regions of large subgrid-scale transfer seem to correlate best with the regions of large-scale energy [Fig. 9(b)]. Such correlations were observed previously[27] for different velocity fields but no convincing physical explanation of this observation is known. The above observations are based on visual inspection of contour plots and thus have a very qualitative character. To evaluate in a more quantitative manner correlations between the subgrid-scale energy transfer and these three quantities a standard correlation coefficient was computed for each case. Its values are -0.24, -0.16, and -0.20 for the large-scale energy, vorticity, and dissipation, respectively. Both the qualitative analysis and the low values of the correlation coefficients clearly illustrate a fairly complex character of interrelations among different physical quantities and give no indications that any simple expression for the subgrid-scale transfer in terms of the resolved energy, enstrophy, or dissipation exists. Meneveau *et al.*[28] recently used a projection pursuit regression algorithm in an attempt to identify in a more systematic manner large-scale physical quantities which could serve to model the subgrid-scale stresses. For isotropic turbulence they were unable to find any large-scale quantity exhibiting significant statistical correlations with the subgrid-scale stresses. Our observations are consistent with this finding.

We conclude from the analysis of the truncated fields that the the subgrid-scale energy transfer is at best marginally correlated with the large-scale energy, enstrophy, and dissipation. This analysis also reveals that the turbulent activity is spatially intermittent and its physical locations are determined by the mutual interactions of the largest scales. The high-wave-number modes in this flow cannot be interpreted as individual, small-scale turbulent eddies, but reflect the presence of steep gradients at the spatial locations determined by the large scales.

The observed importance of the large scales, which constitute only a minute fraction of all spectral modes, in the dynamics of turbulence is encouraging since it suggests that their dynamics may be almost self-contained and thus the accurate subgrid-scale models based on the large-scale velocity information should be possible. The term "almost self-contained dynamics" is not very precise but can be illustrated by the following example. In Fig. 12(a) we plot one plane from the resolved nonlinear transfer field [Eq. (21)] and in Fig. 12(b) the corresponding result for the total nonlinear transfer, i.e., the sum of (21) and (22). It is seen that the spatial structure of the resolved nonlinear transfer is highly correlated with the structure of the total nonlinear transfer. In that sense the dynamics of the large resolved scales, which involves interactions with all modes in the system (the total transfer) is "almost" the same as the internal nonlinear dynamics of the large scales only (the resolved transfer). The difference between both quantities is of course the subgrid-scale nonlinear transfer (22), which when viewed this way, is a small correction to the resolved transfer needed to obtain the total transfer and to account for the nonconservative character of the entire system.

V. CONCLUSIONS

We have performed a detailed analysis of the effects of the subgrid-scale nonlinear interactions on the energetics of isotropic turbulence. The analyzed turbulent velocity field was obtained from a direct numerical simulation of the Taylor–Green vortex flow. Symmetries of the flow were allowed to reach the spatial resolution in the simulation equivalent to 512^3 mesh points and the Reynolds number $R_\lambda \approx 70$. At this Reynolds number the flow exhibits a beginning of the inertial range dynamics at the lowest wave numbers. However, even these low as well as all higher wave numbers are still dominated by dissipative processes.

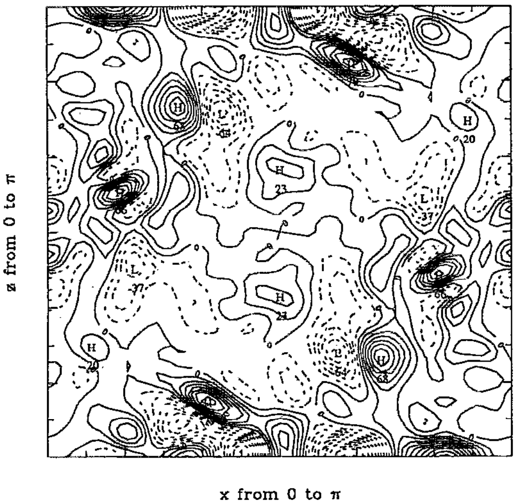

(a)

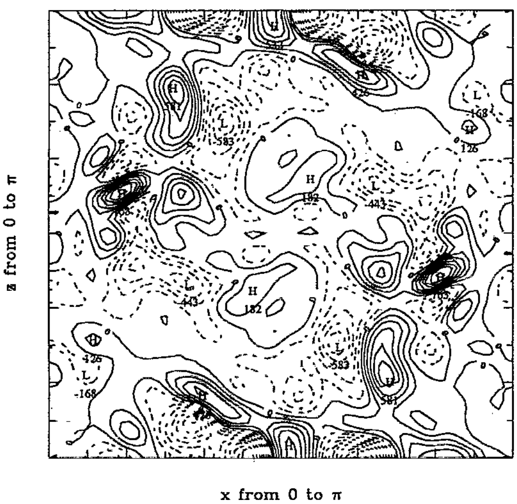

(b)

FIG. 12. The nonlinear energy transfer to/from the resolved modes $k<20$ represented in the physical space: (a) caused by interactions with the resolved modes only (labels scaled by 1000); (b) caused by interactions with the resolved and the unresolved modes (labels scaled by 10 000).

Therefore, while our conclusions are certainly valid for the disspation range dynamics it is less certain that they are applicable to the inertial range dynamics.

An important feature of the computed subgrid-scale energy transfer, in both spectral and physical space representation, is the presence of significant inverse energy transfers, from the unresolved to the resolved scales. The inverse subgrid-scale transfer was predicted and observed before in the context of spectral dynamics of homogeneous turbulence[4,6,11,8] and in the physical space for homogeneous and wall-bounded turbulent flows.[7,27,9,23] The observed significance of the inverse transfer in the energetics of the resolved scales implies that successful subgrid-scale models should properly account for such effects. At the present time these effects are rarely taken into account in the subgrid-scale modeling procedures. If accounted for they are modeled by either adding a random force to the subgrid-scale equations[7,8] or extrapolating from the dynamics of the resolved scales.[9] Since most of the subgrid-scale transfer observed in this work is caused by interactions among highly correlated modes on both sides of the cutoff wave number, approximating effects of such interactions by random forces is debatable. An approach used in the dynamic subgrid-scale model[9] seems more appropriate but it suffers from modeling the inverse transfer by a diffusion-type term with a negative diffusion coefficient, mathematically an inherently unstable situation. It appears that alternate ways of the subgrid-scale modeling which overcome these conceptual and mathematical difficulties should be explored.

Our analysis also reveals that the nonlinear dynamics of the resolved modes with wave numbers $k<k_c$ is governed almost exclusively by their interactions with a limited range of modes with wave numbers not exceeding $2k_c$ and nonlocal, eddy-viscosity-type energy transfer is not observed. Thus, in agreement with the classical picture of the turbulence dynamics,[26] the large scales of a turbulent flow determine the energy flux down the spectrum and the small scales play an entirely passive role by adjusting themselves in such a way as to accommodate this energy flux prescribed by the large scales.

The physical space energy, enstrophy, and dissipation have been computed for the full and truncated velocity fields and compared with the subgrid-scale energy transfer for the same truncation wave number. Surprisingly, these physical quantities computed for both full and truncated fields show many similar spatial features despite the fact that the truncated field contains only 0.16% of all modes present in the system. This result reinforces our conclusion about the dominant role played by the very largest scales in the dynamics of the flow. The level of correlation between these quantities and the subgrid-scale transfer varies from weak for the enstrophy and dissipation, to moderate for the energy.

ACKNOWLEDGMENTS

This research was supported by AFOSR Contract No. 90-0300. The numerical simulations were performed at the Air Force Supercomputer Center, Kirtland AFB.

[1] R. S. Rogallo and P. Moin, "Numerical simulation of turbulent flows," Annu. Rev. Fluid Mech. 16, 99 (1984).
[2] M. Lesieur, *Turbulence in Fluids*, 2nd ed. (Martinus Nijhoff, Dordrecht, The Netherlands, 1990).
[3] J. Smagorinsky, "General circulation experiments with the primitive equations," Mon. Weather Rev. 93, 99 (1963).
[4] R. H. Kraichnan, "Eddy viscosity in two and three dimensions," J. Atmos. Sci. 33, 1521 (1976).
[5] J. Chollet and M. Lesieur, "Parametrization of small scales of three-dimensional isotropic turbulence utilizing spectral closures," J. Atmos. Sci. 38, 2767 (1981).
[6] D. C. Leslie and G. L. Quarini, "The application of turbulence theory to the formulation of subgrid modelling procedures," J. Fluid Mech. 91, 65 (1979).
[7] C. E. Leith, "Stochastic backscatter in a subgrid-scale model: Plane shear mixing layer," Phys. Fluids A 2, 297 (1990).

[8]J. R. Chasnov, "Simulation of the Kolmogorov inertial subrange using an improved subgrid model," Phys. Fluids A **3**, 188 (1991).
[9]M. Germano, U. Piomelli, P. Moin, and W. H. Cabot, "A dynamic subgrid-scale eddy viscosity model," Phys. Fluids A **3**, 1760 (1991).
[10]R. A. Clark, J. H. Ferziger, and W. C. Reynolds, "Evaluation of subgrid-scale models using an accurately simulated turbulent flow," J. Fluid Mech. **91**, 1 (1979).
[11]J. A. Domaradzki, R. W. Metcalfe, R. S. Rogallo, and J. J. Riley, "Analysis of subgrid-scale eddy viscosity with use of results from direct numerical simulations," Phys. Rev. Lett. **58**, 547 (1987).
[12]S. A. Orszag, "Numerical simulation of incompressible flows within simple boundaries. I. Galerkin (spectral) representations," Stud. Appl. Math. **50**, 293 (1971).
[13]G. I. Taylor and A. E. Green, "Mechanism of the production of small eddies from large ones," Proc. R. Soc. London Ser. A **158**, 499 (1937).
[14]M. E. Brachet, D. I. Meiron, S. A. Orszag, B. G. Nickel, R. H. Morf, and U. Frisch, "Small-scale structure of the Taylor–Green vortex," J. Fluid Mech. **130**, 411 (1983).
[15]M. E. Brachet, "The geometry of small-scale structures of the Taylor–Green vortex," C. R. Acad. Sci. Paris **311**, 775 (1990).
[16]S. Kida, "Three-dimensional periodic flows with high-symmetry," J. Phys. Soc. Jpn. **54**, 2132 (1985).
[17]S. Kida and Y. Murakami, "Kolmogorov similarity in freely decaying turbulence," Phys. Fluids **30**, 2030 (1987).
[18]K. Ohkitani and S. Kida, "Triad interactions in a forced turbulence," Phys. Fluids A **4**, 794 (1992).
[19]A. S. Monin and A. M. Yaglom, *Statistical Fluid Mechanics* (MIT Press, Cambridge, MA, 1979).
[20]J. A. Domaradzki, "Nonlocal triad interactions and the dissipation range of isotropic turbulence," Phys. Fluids A **4**, 2037 (1992).
[21]J. A. Domaradzki and R. S. Rogallo, "Energy transfer in isotropic turbulence at low Reynolds numbers," in *Proceedings of the 1988 Summer Program* (Center for Turbulence Research, NASA Ames/Stanford University, Stanford, CA, 1988), CTR-S88, p. 169.
[22]J. A. Domaradzki and R. S. Rogallo, "Local energy transfer and nonlocal interactions in homogeneous, isotropic turbulence," Phys. Fluids A **2**, 413 (1990).
[23]U. Piomelli, W. H. Cabot, P. Moin, and S. Lee, "Subgrid-scale backscatter in turbulent and transitional flows," Phys. Fluids A **3**, 1766 (1991).
[24]M. Lesieur and R. S. Rogallo, "Large-eddy simulation of passive scalar diffusion in isotropic turbulence," Phys. Fluids A **1**, 718 (1989).
[25]P. K. Yeung and J. G. Brasseur, "The response of isotropic turbulence to isotropic and anisotropic forcing at the large scales," Phys. Fluids A **3**, 413 (1991).
[26]G. K. Batchelor, *The Theory of Homogeneous Turbulence* (Cambridge University Press, Cambridge, 1953), p. 113.
[27]J. A. Domaradzki, R. S. Rogallo, and A. A. Wray, "Interscale energy transfer in numerically simulated homogeneous turbulence," in *Proceedings of the 1990 Summer Program* (Center for Turbulence Research, NASA Ames/Stanford University, Stanford, CA, 1990), p. 319.
[28]C. Meneveau, T. S. Lund, and P. Moin, "Search for subgrid scale parametrization by projection pursuit regression," in *Proceedings of the 1992 Summer Program* (Center for Turbulence Research, NASA Ames/Stanford University, Stanford, CA, 1992).